



# A study on the preparation of passivating surface using bi-layer of nanostructured ZnO and silane functionalized polymer: an alternate option to chromate passivating coating

Ashok Kumar Gupta, Suryakanta Nayak, Rakesh S. Moirangthem, T. Venugopalan,  
A. N. Bhagat, Tapan Kumar Rout

Received: 11 May 2021 / Revised: 16 November 2021 / Accepted: 20 November 2021  
© American Coatings Association 2022

**Abstract** A novel bilayer coating was developed over flat steel surface using a simple solution dipping method. Zinc oxide nanostructure (ZnO-NS) on the surfaces of flat steel was grown by chemical treatment with zinc nitrate hexahydrate [ $\text{Zn}(\text{NO}_3)_6 \cdot 6\text{H}_2\text{O}$ ] and hexamethylenetetramine (HMTA,  $\text{C}_6\text{H}_{12}\text{N}_4$ ) in aqueous solution, followed by a thin-layer deposition of amine-terminated poly-dimethylsiloxane (PDMS- $\text{NH}_2$ ). We noticed surface passivation, surface hydrophobicity, and anti-corrosion properties by this robust bilayer concept where both chemical and physical effects were present. The surface properties were measured by contact angle and scanning electron microscope. This nanostructured grown mild steel, i.e., cold-rolled closed annealed steel, was compared with nanostructure grown over zinc-coated steel, i.e., galvanized and galvanized iron. Different flat-coated specimens were characterized by Fourier transform infrared spectroscopy. The formation of ZnO-NS on steel substrate was confirmed by XRD analysis. The corrosion behavior of the different specimens was also

studied through DC polarization and electrochemical impedance spectroscopy. An excellent intact bilayer coating was proposed in the interest of structural and automotive applications.

**Keywords** Hydrophobic, Silane, Zinc oxide, Polymer, PDMS, Passivation, Corrosion

## Introduction

Hydrophobic material surfaces have water repellent property with a high-water contact angle ( $\text{WCA} > 90^\circ$ ), which helps to prevent the absorption of water molecules on the surface. The naturally occurring lotus leaf has surface hydrophobicity and self-cleaning behavior due to the presence of micro/nanostructured surface. The water droplets on the lotus leaf surface presume a spherical shape having minimum surface energy and roll off the surface, collecting all the dirt particles on the way and providing self-cleaning property to the lotus leaf surface. This is known as “lotus leaf effect.”<sup>1–4</sup> Many researchers have been inspired by this characteristic of the lotus leaf to develop super-hydrophobic coatings.<sup>5–7</sup> A nanostructured surface with low-surface energy coating solution can produce a hydrophobic surface with higher WCA.<sup>8</sup> Many attempts have been made to develop roughness on the surface using different nanomaterials (nanostructured flakes, nanorods, and nanospheres)<sup>9–11</sup> and processes (electroless replacement deposition process,<sup>12, 13</sup> surface etching with HF,<sup>14, 15</sup> sol-gel method,<sup>16</sup> and precipitation method<sup>17</sup>). Hydrophobic surfaces have self-cleaning, oil repellency behavior and they also protect from adhesion of bacterial activities.<sup>18</sup> Various researchers have worked on various hydrophobic coatings which involve a solution of PDMS and TEOS. Jing Zhao et al. have developed hydrophobic materials for the consolidation of damaged pottery using hybrid

---

Ashok Kumar Gupta and Suryakanta Nayak contributed equally to this work.

---

A. K. Gupta  
Cold Rolling Mill (CRM), Tata Steel Limited, Jamshedpur  
831 001, India

S. Nayak, A. N. Bhagat, T. K. Rout (✉)  
R & D, Surface Engineering Research Group, Tata Steel  
Limited, Jamshedpur 831 001, India  
e-mail: tapankumarout@tatasteel.com

R. S. Moirangthem  
Department of Applied Physics, Indian Institute of  
Technology Dhanbad, Jharkhand 826 004, India

T. Venugopalan  
Indian Institute of Technology Madras, Chennai, Tamil  
Nadu 600 036, India

mixture of TEOS and PDMS-OH.<sup>19</sup> Gong and He et al. have developed a superhydrophobic nanocomposite surface using PDMS and hydrophilic/hydrophobic silica nanoparticles. The developed surface has high WCA of 156.4° and a sliding angle of less than 5°. This coating can be applied on various substrates like paper, glass, and plastic. They have proven this superhydrophobic surface to be suitable for self-cleaning and antifouling.<sup>20</sup> Guan et al. have prepared hydrophobic coating on paper using TEOS and PDMS. It is observed by them that the silica nanoparticles obtained by the hydrolysis of TEOS, improved the transparency of the paper and thermal stability of the coating.<sup>21</sup> Hasanzadeh et al. have fabricated a superhydrophobic and breathable fabric using amino-modified PDMS and silica nanoparticles. Here, the textile fabrics were coated with silica nanoparticles (prepared from TEOS) to obtain enough roughness with hydrophobic surface chemistry. Then, these coated fabrics were treated with PDMS and aminopropyltriethoxysilane (APTES) to reduce the surface energy.<sup>22</sup> Chui Wan Tsen et al. have studied on the deposition of polymer multilayers on free-standing ZnO tetrapods, ZnO tetrapods on a substrate, and ZnO nanorod arrays. They also have attached “Au” nanoparticles on ZnO nanostructure surface using layer-by-layer deposition which is observed by high-resolution transmission electron microscopy. The optical and electrical properties of polymer-ZnO nanostructures were varied by simply changing the polymer for deposition. Similarly, other properties can be varied by increasing the polymer thickness by increasing the number of polymer layers.<sup>23</sup> Many researchers have used vinyl-terminated PDMS (V-PDMS) on a ‘Cu’ deposited rough surface and use of PTFE with PDMS to form hydrophobic surface. Many of them have used silica particles to increase hydrophobicity along with silanes and in some methods, fluorinated compounds have also been used.<sup>24, 25</sup> These processes are found to be complex, expensive, time consuming, and have negative environmental effects. There is requirement to develop a method that is simple and environmental friendly.

The present work is carried out to develop a hydrophobic surface by a simple technique using ZnO-nano structure (ZnO-NS) for creating surface roughness with a thin passivating film of PDMS-NH<sub>2</sub>/TEOS to further increase the hydrophobicity (contact angle) of the metal surface. The ZnO-NS was obtained by solution dipping method using zinc nitrate hexahydrate and HMTA and the details are given in “Preparation of ZnO-NS on steel surfaces (GA, GI, and CRCA)” section. After the formation of ZnO-NS on steel surface, it was further coated with silica coating solution, obtained from PDMS-NH<sub>2</sub> and TEOS (details given in “Coating solution preparation” section).

## Experimental section

### Materials used

Poly(dimethylsiloxane), bis(3-aminopropyl)-terminated (PDMS-NH<sub>2</sub>) tetraethyl orthosilicate (TEOS), Zinc nitrate hexahydrate [Zn(NO<sub>3</sub>)<sub>6</sub>·6H<sub>2</sub>O], and hexamethyltetraamine (HMTA) were procured from Sigma-Aldrich, India. Isopropyl alcohol and acetylacetone (AcAc) were procured from Fisher Scientific, India. Distilled water was used as solvent for the synthesis of coating solutions. Galvannealed (GA), galvanized (GI), and mild steel (CRCA) substrate samples were provided by Tata Steel, Jamshedpur, India. The details about the sample specimens are listed in Table 1. Chromated GA/GI samples were collected from Tata Steel, Jamshedpur, India for comparative study.

### Preparation of ZnO-NS on steel surfaces (GA, GI, and CRCA)

An aqueous solution of 100 mL with 50 mM concentration (by weight percentage) was prepared using zinc nitrate hexahydrate and HMTA dissolved in distilled water. This mixture was stirred continuously while heating at 80°C for 1 h and then it was filtered. The samples of GA, GI, and CRCA were cleaned by hot alkali solution. The cleaned steel samples were immersed in the above prepared solution for 9–10 min and heated at 90°C. Further, these samples were processed through annealing furnace at 450°C for 1–2 s followed by slow cooling. The surface morphology and chemical characterization of developed ZnO-NS were analyzed by SEM and EDS, respectively. The thickness of ZnO-NS was measured by a coating thickness gauge (PosiTector® 6000) and thickness was found to be 7–8 μm.

### Coating solution preparation

PDMS-NH<sub>2</sub> and TEOS were used for the preparation of the coating solution. First, 50 mL of isopropyl alcohol was taken in a beaker and was stirred at 170 rpm by a magnetic stirrer. Next, 6 mL of PDMS-NH<sub>2</sub> was added dropwise to the above IPA followed by the dropwise addition of 6 mL of TEOS. Then, 1 mL of distilled water was added into the above solution dropwise. Finally, 1 mL of acetylacetone was added to prevent the solution from precipitating. The above solution was kept on stirrer for 3 h and final coating solution was found to be clear solution with pH range of 9–10.

**Table 1: Details about substrates used for the preparation of different specimens**

S. No.	Substrate	Description
1	CRCA: Cold-Rolled Closed Annealed	Mild steel doped with ZnO
2	GA: Galvannealed steel	10% Fe-Zn alloy layer over mild steel
3	GI: Galvanized iron	100% Zn layer over mild steel

Mild Steel Chemistry: C-0.04; Mn-0.40; Si-0.04; S-0.02; P-0.035; Al- 0.02; N-70ppm; YS-350; UTS-410; EL-32

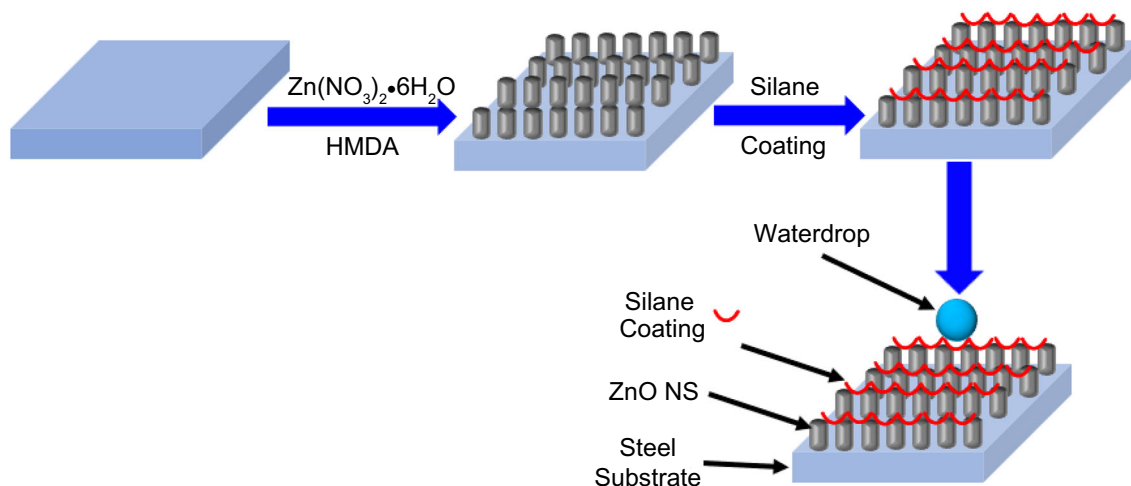


**Fig. 1: Schematic representation for the preparation of ZnO nanostructure and silane coating on the surfaces of GA, GI, and CRCA substrates**

### Coated sample/specimen preparation

Both bare and nanostructured (NS) steel samples (GA, GI, and CRCA) were dip coated by the above coating stock solution with a dipping time of 30–40 s and finally cured in the oven for 2 min at 100°C. Then, the dried samples were taken for different characterization. The dry film thickness of silane coating was around 2–3 µm. Fig. 1 shows the schematic representation for the preparation of ZnO nanostructure and silane coating on the surfaces of GA, GI, and CRCA substrates. The possible reaction mechanism between PDMS-NH<sub>2</sub> and TEOS is shown in Fig. 2.

### Characterizations

The microstructural properties of coated steel samples were evaluated by scanning electron microscope (SEM-Nova NanoSEM 450) equipped with energy-dispersive spectrometer (EDS). Both bare and NS-steel samples were uniformly coated with gold layer to make them conductive and avoid any charging during the SEM operation. The FTIR spectra of coated samples were recorded on a Fourier transform infrared

spectrophotometer (Bruker, model VERTEX 80V) in the spectra range of 400–4000 cm<sup>-1</sup>. The sessile drop method was used for the measurement of contact angle. The static contact angle of coated sample was determined by contact angle system (OCA 15EC, DataPhysics Instrument, Filderstadt, Germany). Demineralized (DM) water was used as testing liquid. The corrosion resistance properties of both bare and coated steel substrates were investigated by potentiodynamic polarization and electrochemical impedance spectroscopy (EIS) test (Gamry 3000). The EIS study was carried out in the frequency range of 0.01 Hz to 100 kHz. A three-electrode system was used for this test where the samples act as the working electrode (1 cm<sup>2</sup> of exposed area), saturated calomel electrode (SCE) as reference, and graphite was used as a counter electrode. In all the measurements, 3.5% aqueous NaCl solution was used as an electrolyte. The phase formation and crystallographic state of coated samples were determined by an X-ray diffractometer (XRD, PANalytical Xpert Pro diffractometer). The diffractograms were scanned in the 2θ range from 10 to 80 at a rate of 3/min. Confocal laser scanning microscopy (CLSM, Olympus Lext OLS4100) was used to check the surface roughness of the coated samples.

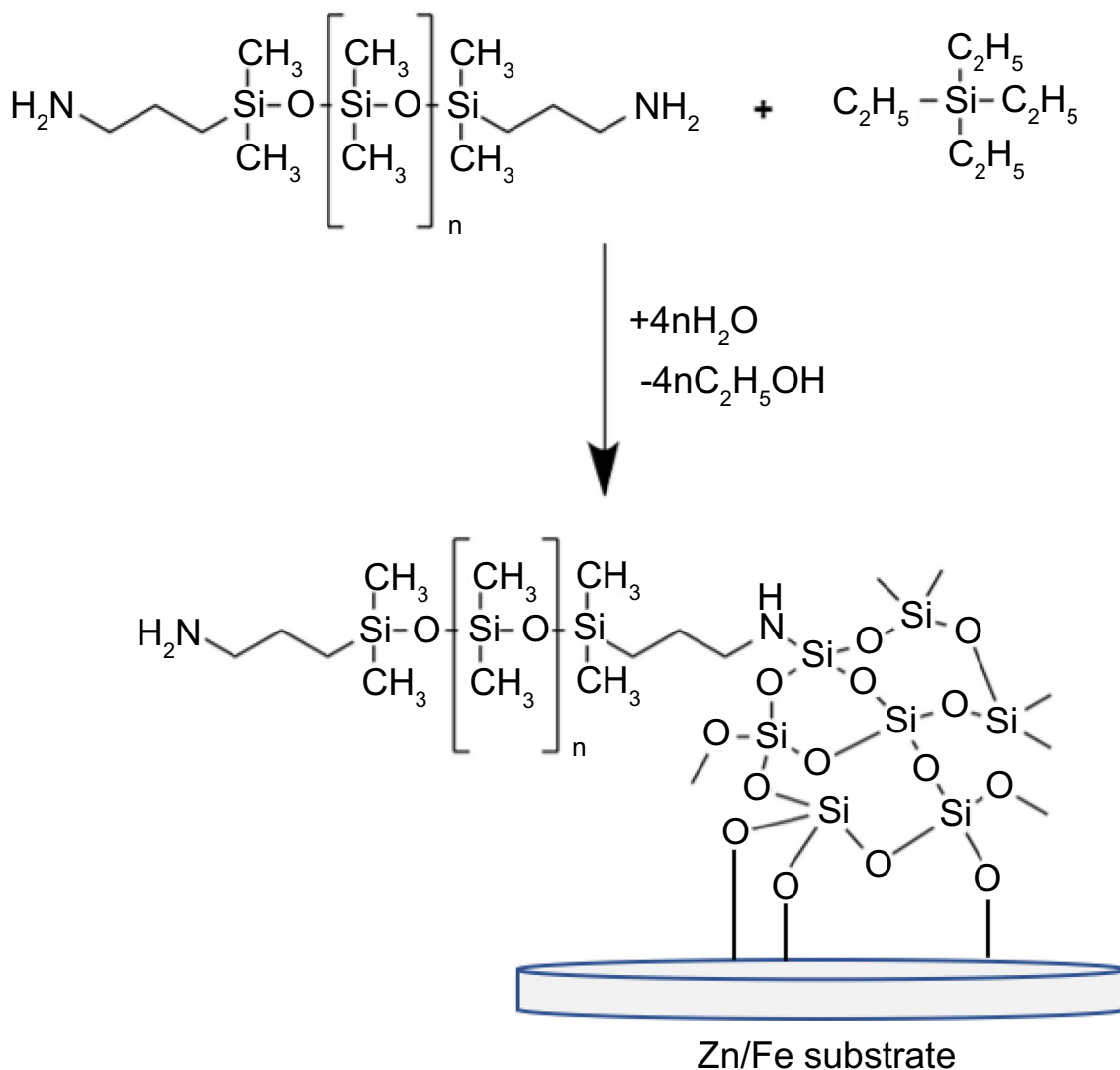


Fig. 2: Possible reaction mechanism between PDMS-NH<sub>2</sub> and TEOS

## Results and discussion

### Scanning electron microscopy (SEM) study

Figure 3 shows the scanning electron microscopy images of both bare and nanostructured (NS) steel samples of GA, GI, and CRCA. It was observed from the SEM micrographs that the ZnO nanostructures (NS) are developed on the surface of GA, GI, and CRCA samples (Fig. 3b, d, f). We observed highly hexagonal ZnO nanostructures generated across large areas under solution treatment (mentioned under methodology) on galvanized steel substrates and CRCA substrate (mild steel doped with ZnO). The nanostructures were inhomogeneously distributed over the surface having diameters from  $\sim 100$  to  $400$  nm and are several micrometers long. The nanostructures were well-adhered to the underlying steel substrates, which enables the preparation of robust substrate-integrated

ZnO nanostructure arrays suitable for the use in anti-corrosion layer as a replacement to hexavalent chromate passivation coating. This ZnO nanostructure was further treated with silane solution (mentioned under methodology) to ensure its robustness against wear resistance and de-wettability of water by enhancing hydrophobicity. The bilayer concept has been used for the anti-corrosion as described below. It has been seen earlier for the growth of ZnO nanostructures by several methods namely carbothermal growth of ZnO nanowires, ZnO nanowire growing from a fractured island of Zn; vaporized Zn species using physical vapor deposition (PVD) set up, and growth in an ambient open-air yields networks of ZnO tetrapods using tubular furnace.<sup>26</sup> But, we have generated by a simple solution dipping method followed by thermal annealing, which can be used on the industrial scale. The grown ZnO nanostructures are of solid hexagonal rod with smooth tips and there are no sharp edges. The



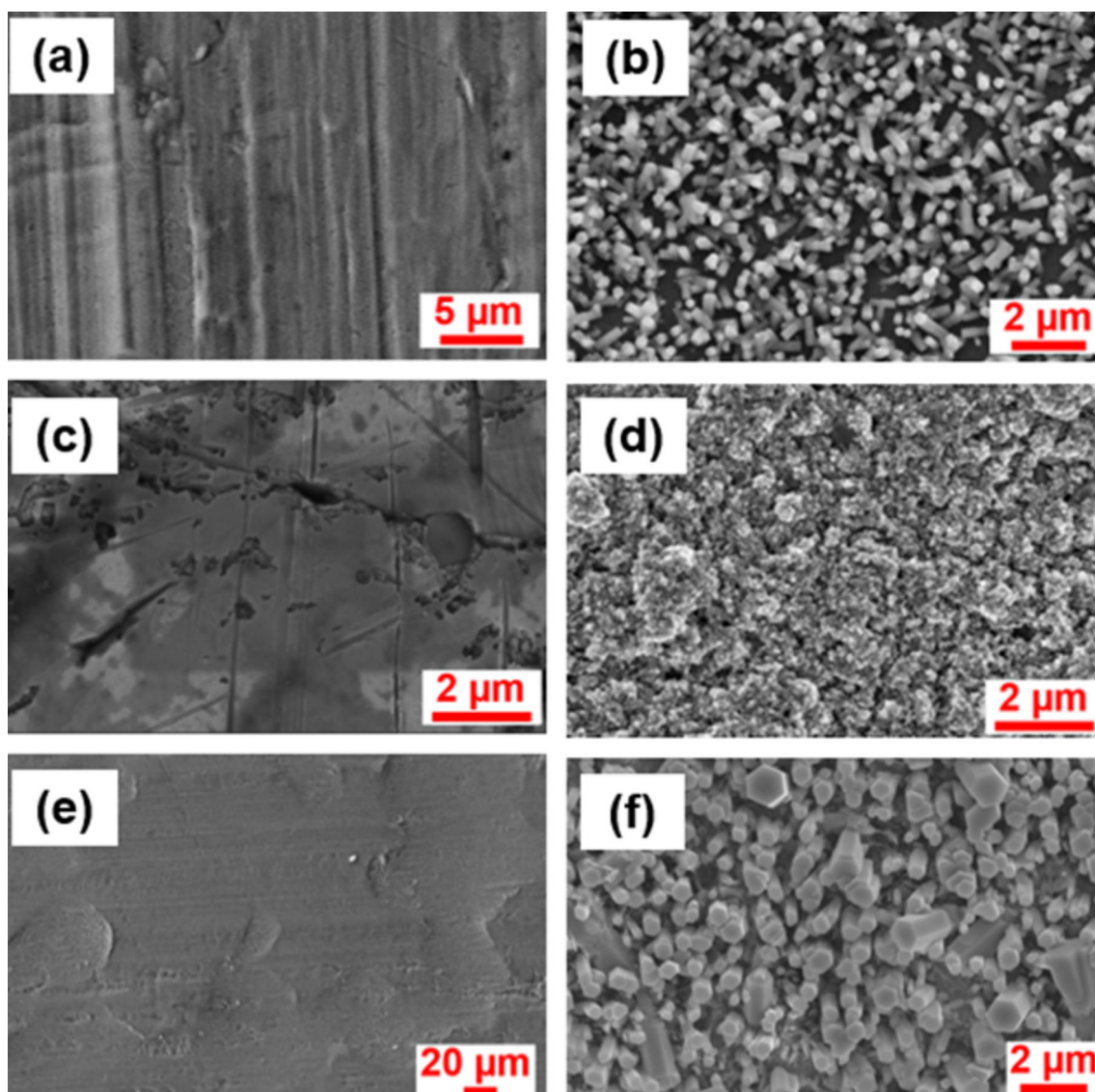


**Fig. 3:** Scanning electron microscopy images of both bare (a, c, e) and nanostructured (b, d, and f) GA, CRCA, and GI steels

elemental composition of the coating on the flat samples was evaluated by the energy-dispersive X-ray spectroscopy (EDS). In the case of EDS, the samples are scanned at 5000 $\times$  magnification. Table 2 shows the weight % and atomic % of the elements present on the surface of coated samples.

From Table 2, the presence of basic elements in bare GA (presence of Fe and Zn), GI (presence of Zn element), and CRCA were noted. The corresponding EDS spectra are given in Figs. 4-6. The selected area was analyzed under EDS. The different samples can be clearly distinguished from each other. In the case of GA sample, Zinc concentration has increased from  $\sim 46\%$  (bare coated) to  $\sim 83\%$  (GA-NS); similarly, in the case of GI, zinc concentration has increased from  $\sim 54\%$  (bare coated) to  $\sim 85\%$  (GI-NS) and  $\sim 0.0\%$  (bare coated) to  $\sim 2.82\%$  (CRCA-NS) for the mild steel. We observed Si concentrations of  $\sim 9\%$ ,  $\sim 33\%$

and  $\sim 12\%$  after dipping into amine-terminated silane stuck solution for obtaining a thin film coating over GA-NS, GI-NS, and CRCA-NS, respectively. The presence of “Si” along with the basic elements shows the presence of silane coating on the steel surface which can help to further improve the surface properties chemically in terms of hydrophobicity.

#### *X-ray diffraction analysis*

X-ray diffraction (XRD) analysis was done on ZnO nanostructured (NS) steel samples (Fig. 7). The diffraction peaks of ZnO-NS are observed at  $2\theta = 31.84^\circ, 34.41^\circ, 36.21^\circ, 47.63^\circ, 56.66^\circ, 62.91^\circ, 66.52^\circ, 68.08^\circ, 69.15^\circ, 72.92^\circ, \text{ and } 76.96^\circ$ , and these peaks represent the Bragg reflections from the (100), (002), (101), (102), (110), (103), (200), (112), (201), (004), and

**Table 2: EDS elemental composition of different coated samples**

Element	GA-Si coated		GI-Si coated		CRCA-Si coated		GA-NS		GI-NS		CRCA-NS		GA-NS Si-Coated		GI-NS Si-Coated		CRCA-NS Si-Coated	
	W %	A%	W %	A%	W %	A%	W %	A%	W %	A%	W %	A%	W %	A%	W %	A%	W %	A%
O K	14.21	32.22	17.62	37.64	10.94	25.64	4.58	15.91	7.84	24.53	18.64	44.37	9.91	27.41	29.82	50.63	18.16	39.90
Al K	1.89	2.54	2.10	2.65	1.55	2.16	1.06	2.17	4.18	7.75	0.41	0.58	2.24	3.68	2.53	2.54	0.95	1.23
Si K	23.55	30.42	25.55	31.09	20.23	27.01	***	***	***	***	0.18	0.25	9.24	14.57	33.93	32.81	12.93	16.18
Fe K	14.00	9.09	***	***	67.28	45.19	11.37	11.32	2.80	2.51	77.94	53.15	9.53	7.55	***	***	66.88	42.10
Zn K	46.35	25.72	54.73	28.61	0.005	0.013	83.00	70.60	85.18	65.22	2.82	1.64	69.08	46.78	33.72	14.01	1.09	0.59

\*W%, Weight%, A%, Atomic%

\*\*\*NIL

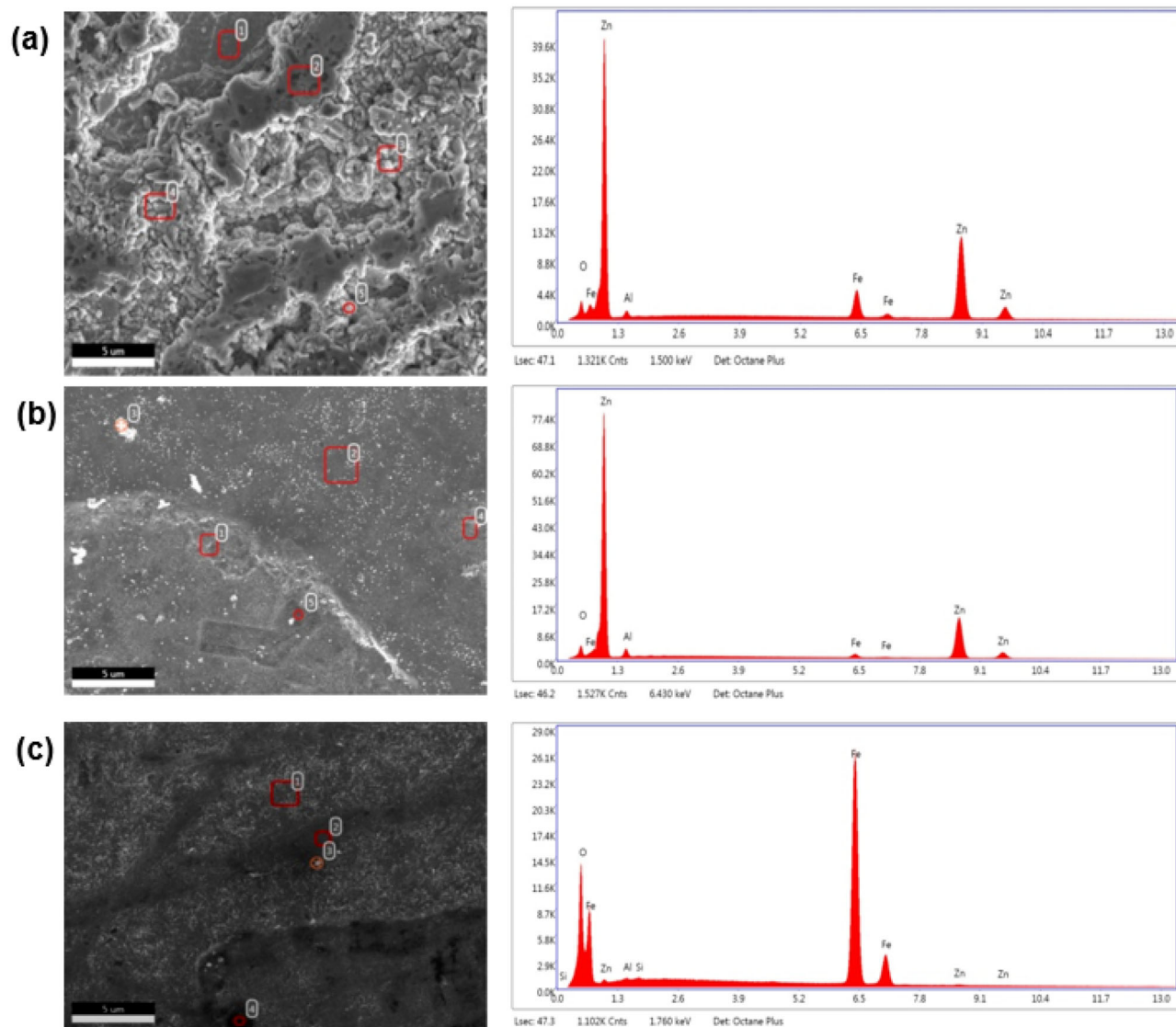


**Fig. 4:** Energy-dispersive X-ray spectroscopy (EDS) of bare (a) GA-Si coated, (b) GI-Si coated, and (c) CRCA-Si coated samples

(202) planes, respectively.<sup>27</sup> So, it confirmed the presence ZnO-NS on the steel surface. There is also some impurity/unknown peak observed.

#### **Fourier transform infrared (FTIR) spectroscopy**

Figure 8a and b show the FTIR spectra of PDMS-NH<sub>2</sub> precursor and TEOS precursor, respectively. Figure 8c shows the FTIR spectra of different coated steel samples (GA, GI, and CRCA) and Fig. 8d shows the FTIR spectra of different coated nanostructured steel samples (GA, GI, and CRCA).

We observed from Fig. 8a that PDMS-NH<sub>2</sub> has the peak positions at 2969.91 and 3349.11 cm<sup>-1</sup> that correspond to the -CH and -NH<sub>2</sub> stretching frequency, respectively, and other peaks correspond to the usual

peaks for PDMS polymer [791.52 cm<sup>-1</sup> (-CH<sub>3</sub> rocking and Si-C stretching in Si-CH<sub>3</sub>), 1013.15 and 1087.01 cm<sup>-1</sup> (Si-O-Si stretching), 1264.29 cm<sup>-1</sup> (CH<sub>3</sub> deformation in Si-CH<sub>3</sub>)].<sup>28, 29</sup> We also found from Fig. 8b that TEOS has the peak positions at 470.58, 786.59, 1077.15, and 2979.75 cm<sup>-1</sup> that correspond to -O-Si-O, -O-Si-CH<sub>3</sub> (Si-O bending), Si-O-Si, and -CH<sub>3</sub> stretching frequencies, respectively. The band at 958.96 cm<sup>-1</sup> corresponds to the stretching vibrations of Si-O-H.<sup>30–33</sup> When we mixed these two precursors and applied on flat samples by dipping, the coated flat samples thus obtained are shown in Fig. 8c and d which indicate the reaction happened between PDMS-NH<sub>2</sub> and TEOS to form the hydrophobic coating (mentioned in the contact angle section). A chemical reaction between these two precursors has been put forward in Fig. 2. Therefore, it is ascertained that the -Si-NH bond was

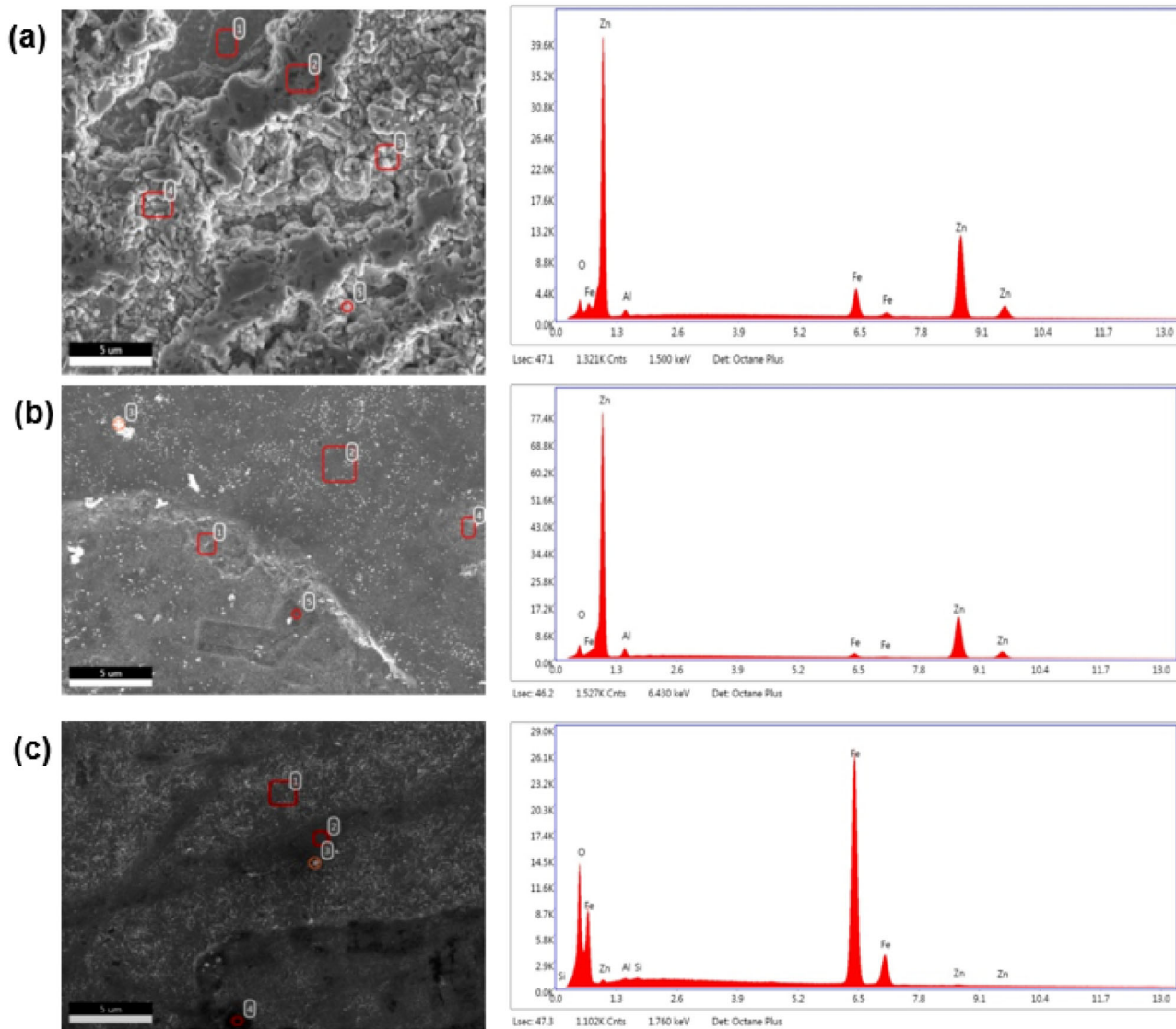


Fig. 5: Energy-dispersive X-ray spectroscopy (EDS) of (a) GA-NS, (b) GI-NS, and (c) CRCA-NS sample

formed after the reaction between PDMS-NH<sub>2</sub> and TEOS. It is also evident by the presence of a peak at 863 cm<sup>-1</sup>.<sup>34</sup>

**Contact angle measurement**

The contact angle measurement was carried out to evaluate the hydrophobicity, wetting behavior, and the free surface energy of both types the flat (GA/GI/CRCA) sample surfaces. The contact angle measurement was done for all GA, GI, and CRCA samples (bare, coated, and NS-coated steel sheets), and the images are shown in Fig. 9. It is observed that there was an increase in contact angle for each type of sample (GA/GI/CRCA) after the amine-terminated silane

coating application. However, there was a significant increase in contact angle in the case of coated sheets with ZnO nanostructure (NS). The presence of ZnO nanostructure on the flat steel surface reduces the surface energy, thereby decreasing the water droplet’s adhesion to the surface. Due to the manifestation of these nanostructure patterns on the surface, dirt particles can be removed along with water droplets giving the surface a self-cleaning behavior. The improvement of surface hydrophobicity in the case of coated samples without nanostructure is due to the presence of non-polar -CH<sub>3</sub> group from amine-terminated silane coupling group (PDMS-NH<sub>2</sub> part). However, further increase in hydrophobicity is due to the existence of ZnO nanostructure on the flat (GA/GI/CRCA) surface.



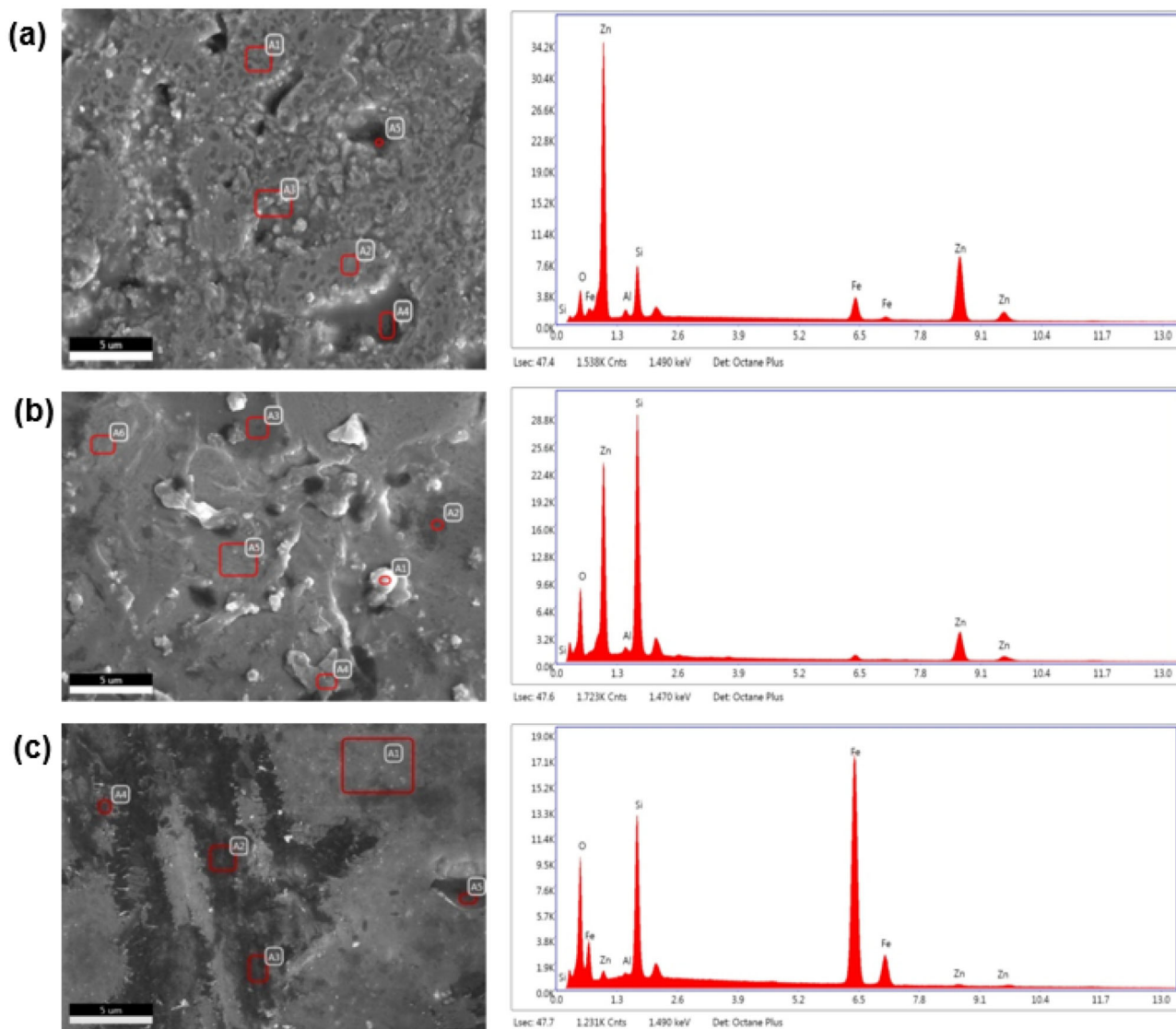


Fig. 6: Energy-dispersive X-ray spectroscopy (EDS) of (a) GA-NS Si-coated, (b) GI-NS Si-coated, and (c) CRCA-NS Si-coated samples

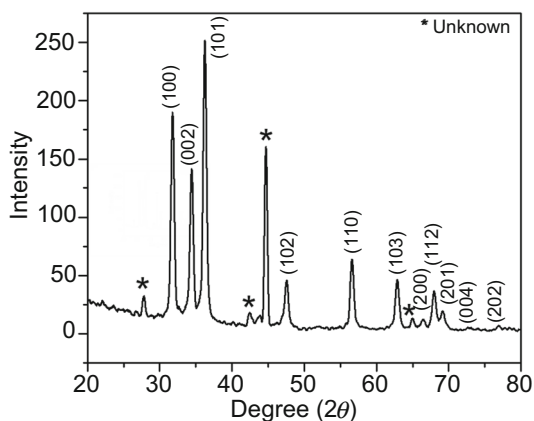
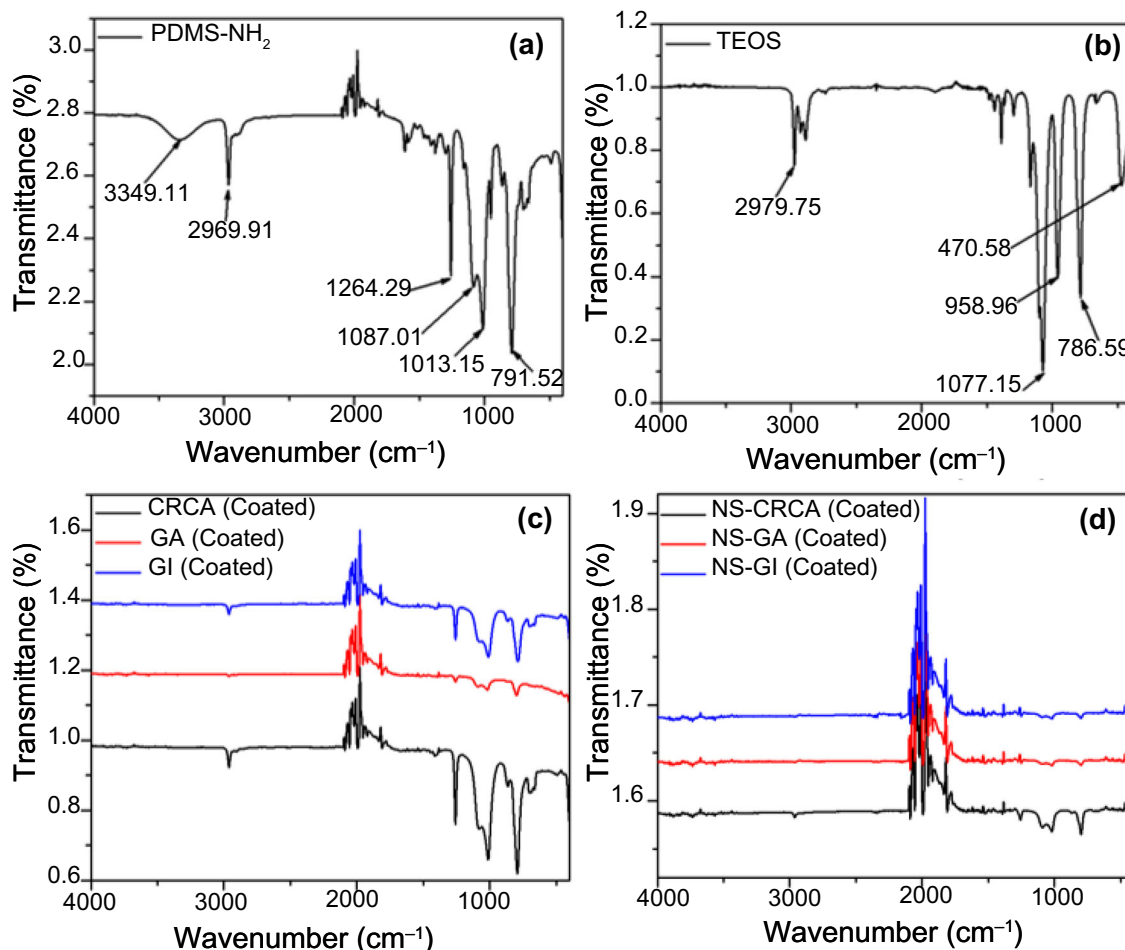


Fig. 7: XRD pattern of the prepared ZnO-NS on the steel surface

### Electrochemical impedance spectroscopy (EIS) study

We used electrochemical impedance spectroscopy (EIS) to evaluate the electrochemical behavior of the coating in 3.5% NaCl solution. This technique is widely employed to understand the interfacial phenomena between bare substrates and coatings to establish a corrosion mechanism and rank the investigated coatings according to their performances. We have evaluated both bare substrates and bilayered nanostructure coated substrates after exposing to 3.5% NaCl at an applied voltage of 10 mV in the frequency range of 0.01 to 10<sup>5</sup> Hz and measured the current response. All these data were plotted between modulus of impedance vs log frequency using Bode theory and hence called Bode plot. This experimental data was fitted by using



**Fig. 8:** FTIR spectra of (a) PDMS-NH<sub>2</sub>, (b) tetraethyl orthosilicate (TEOS), (iii) coating on flat samples (GA, GA, and CRCA). And (d) coating on nanostructured flat samples (GA, GI, and CRCA)

an electrical equivalent circuit model which is a simplified Randles cell model to evaluate different electrical equivalent elements such as solution resistance ( $R_s$ ), coating capacitance ( $C_c$ ), and impedance ( $|Z|$ ). The Bode plot has more advantages over the Nyquist plot, since one can understand from Bode plot how the impedance varies with the frequency but not in Nyquist plot. Coating behavior in terms of resistor and capacitor can be well described in our case by using Randles electrical circuit model (simulation of coating-solution interface) as shown in Fig. 10a.

We could derive values of different electrical circuit elements such as  $R_p$ ,  $C_c$ , and  $R_s$  from the plot of the magnitude of impedance ( $|Z|$ ) on a log scale in y-axis and frequency in x-axis of Bode plot. At high-frequency region (right side) as shown in Fig. 10b, the ohmic resistance dominates the impedance and  $\log(R_s)$  can be recorded from high-frequency horizontal plateau (dotted line intercepting the y-axis). At low-frequency region, both  $\log(R_s + R_p)$  can be recorded by considering the horizontal plateau of the impedance curve. At intermediate frequencies, this impedance curve may have different slopes, if it is a straight line

then the slope will be -1. Extrapolating this line to the  $\log |Z|$  axis at  $\omega = 1$  ( $f = 0.16$  Hz,  $\log \omega = 0$ ), yields the value of coating capacitance ( $C_c$ ) from the given relationship:  $|Z| = 1/C_c$ , where  $\omega = 2\pi f$ . The Bode plot shows the variation of phase angle ( $\theta$ ) with the frequency ( $f$ ). In the low and high-frequency region, behavior of the Randles cell is a resistor, because phase angle is nearly zero on these frequency regions. In the intermediate frequency region, the phase angle ( $\theta$ ) increases as the imaginary component of impedance increases and goes towards higher phase angle indicating capacitive behavior. These components were derived by plotting a curve between the phase angle ( $\theta$ ) vs  $\log f$ , this plot yields a peak at  $\omega$  ( $\theta = \max$ ), the frequency, in radians, at which the phase shift of the response is maximum confirming the simulated electrical circuit transition from ohmic resistance to capacitive behavior. We observed in our study that the frequency ranges between  $10^{-3}$  Hz and  $10^2$  Hz were showing capacitive character. The physical significance of the EIS result in the higher frequency region is also related to both the hydrophobic characteristics of the surface and the coating compactness,

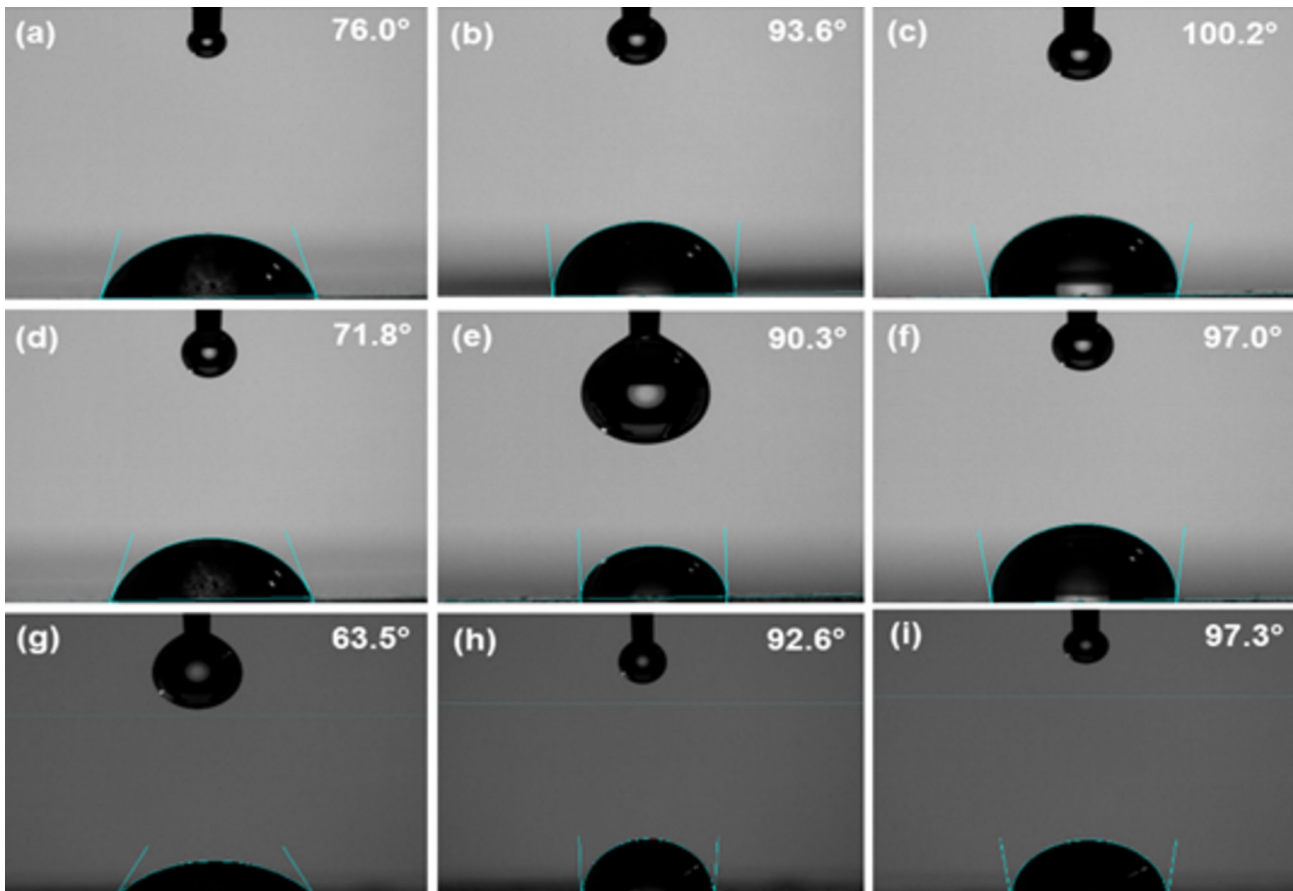


Fig. 9: Contact angle images of (a–c) GA samples (bare, coated, and NS-coated steel sheets, respectively), (d–f) GI samples (bare, coated, and NS-coated steel sheets, respectively), (g–i) CRCA samples (bare, coated, and NS-coated steel sheets, respectively)

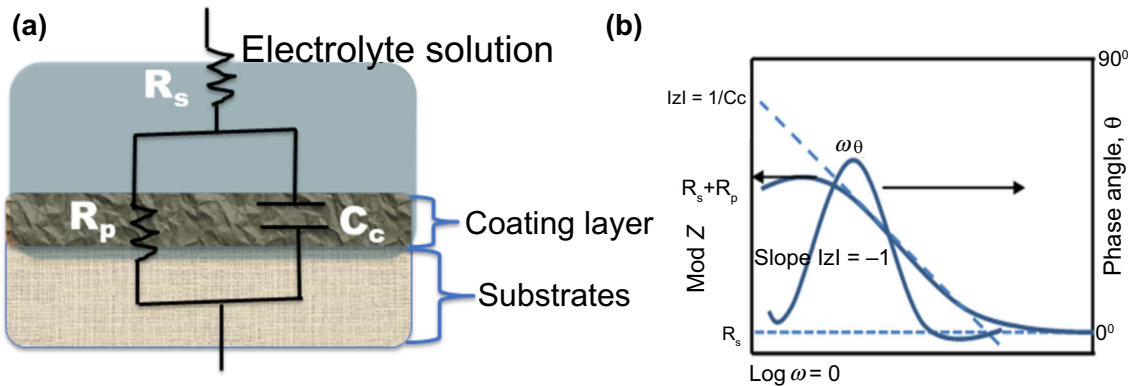


Fig. 10: (a) Electrical circuit model representing coating and substrate interface and (b) schematic Bode plot for deriving different electrical circuit elements values

while low-frequency EIS modulus is associated with the corrosion resistance behavior.<sup>35, 36</sup>

The coating capacitance ( $C_c$ ), polarization resistance ( $R_p$ ), and impedance ( $|Z|$ ) values were derived from the Bode plot by curve fitting (Fig. 11) and are presented in Table 3. It was found that the nanostructured coated NS-CRCA ( $R_p = 3.79 \text{ ohm.cm}^2$ ) shows higher corro-

sion resistance compared to CRCA-coated ( $R_p = 2.46 \text{ ohm.cm}^2$ ). We know polarization resistance is inversely proportional to the corrosion rate ( $R_p \propto 1/\text{corrosion rate}$ ), therefore nanostructured grown CRCA shows higher corrosion resistance than the uncoated one. Similarly, nanostructured coating over GA has shown comparatively higher corrosion resistance NS-GA ( $R_p$

= 3.70 ohm.cm<sup>2</sup>) than the bare GA ( $R_p = 2.86$  ohm.cm<sup>2</sup>), whereas bare GI performs similar to nanostructured NS-GI because polarization resistance ( $R_p$ ) of bare GI (3.05 ohm.cm<sup>2</sup>) was close with polarization resistance of nanostructured NS-GI (2.95 ohm.com<sup>2</sup>). These results are supplemented by coating capacitance values derived from Bode plot where coating capacitance values were found low in the case of nanostructured specimens i.e., NS-CRCA ( $C_c: 0.11 \times 10^{-4}$  F/cm<sup>2</sup>) and NS-GA ( $0.12 \times 10^{-4}$  F/cm<sup>2</sup>) as compared to bare CRCA ( $1.53 \times 10^{-4}$  F/cm<sup>2</sup>) and bare GA ( $1.11 \times 10^{-4}$  F/cm<sup>2</sup>), respectively. This indicated that nanostructured coating is providing barrier to ingress of water and ions into the substrates. The sharp slope (−1) found in the medium frequency range for both NS-GA and NS-CRCA confirmed the good passivating barrier coating to the electrolytes (high  $R_s$ ) by acting as a capacitor, and is made evident by higher modulus of impedance value at lower frequency range.<sup>37</sup> The protection efficiencies of NS coatings over the bare substrates (CRCA, GA, and GI) are 54%, 29%, and 3%, respectively. The protection efficiency was calculated by equation (1) as given below:

$$\text{Protection efficiency} = \frac{R_{pf} - R_{pi}}{R_{pi}} \times 100 \quad (1)$$

where  $R_{pf}$ , final polarization resistance;  $R_{pi}$ , initial polarization resistance.

It was also evident by shifting of phase angle (more than 60°) at higher frequency range from Fig. 11b. The remaining coatings showed shallower slope in the lower frequency range indicative of poor capacitor. This means that electrolyte solutions are penetrating into the coating interface by which phase angle shifting away from 90° and going towards lower values (55°) at medium frequencies. It was confirmed that both the charge transfer reaction, followed by mass transfer,

took place at the coating and solution interface. According to the results, a noticeable decrease in  $C_c$  for the nanostructured coating was an indication of higher passivating behavior therefore higher corrosion resistance. The improvement in the presence of the nanostructured coating clearly resists the water and ionic species due to hydrophobic nature of the composite coating in conjunction with zinc nanorods as shown in Fig. 11. The polarization findings have been strengthened further by the observation of EIS study that the NS-flat samples can effectively delay or suppress the penetration of the corrosive ions of NaCl via the coating and improve the corrosion passivation characteristics.

We did an electrochemical impedance spectroscopy (EIS) comparison study of NS-coated GA/GI samples with chromated GA/GI samples and the result is given in Fig. 12. From the figure, it is observed that NS-coated GI sample has more coating resistance compared to chromated GI sample. However, there is small variation in the case of GA samples.

### Polarization study

We have carried out potentiodynamic measurement at 1.67 mV/s from − 0.5 V to 1.5 V vs SCE for both the flat-coated substrates in order to know the passivation behavior, hence anti-corrosion in 3.5% NaCl solution. The potentiodynamic polarization curve for both bare and nanostructured coated steel samples (GA/GI/CRCA) is shown in Fig. 13.

The cathodic and anodic DC polarization slopes ( $b_c$ ) and ( $b_a$ ) indicated significant variations between the cathodic reduction, mechanisms of anodic dissolution, and the microstructures of tested samples (Table 4). From the comparison, it has been observed that the NS-CRCA and NS-GA potentiodynamic polarization curve showed passivation region in the range of − 0.3

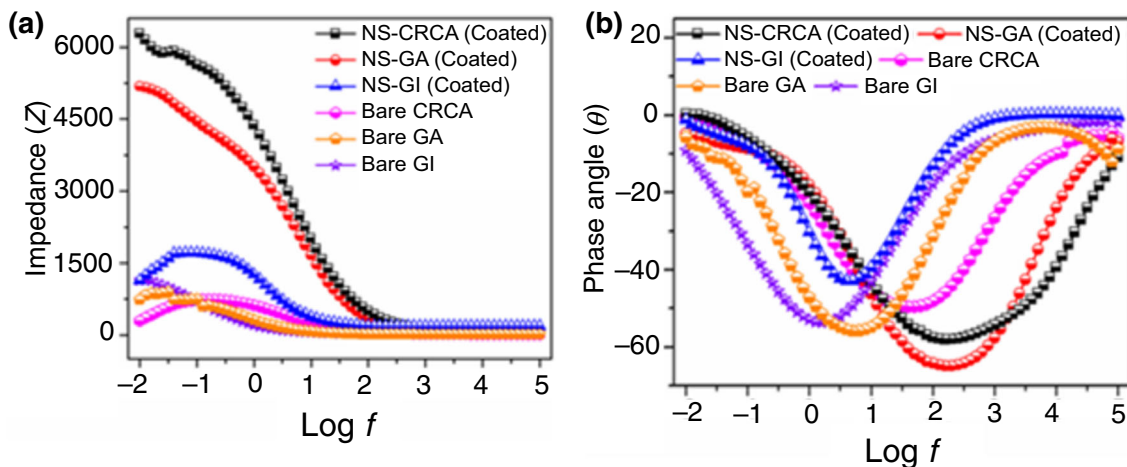
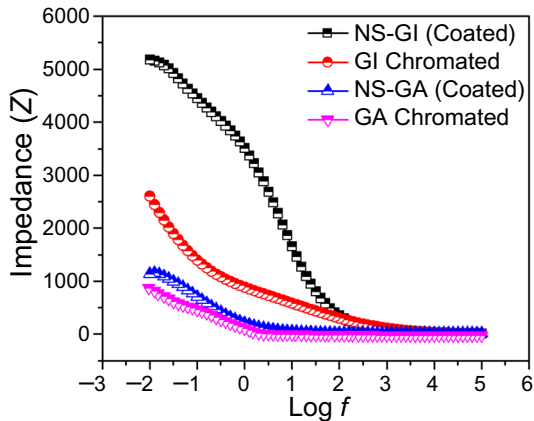


Fig. 11: Electrochemical impedance spectroscopy study on different bare and coated samples in 3.5% NaCl solution; (a) Bode plots for Impedance vs Log f; (b) Bode plots for Phase angle vs Log f



**Table 3: EIS parameters of coated steel substrates during test under 3.5% NaCl solution**

Circuit Element	Bare CRCA	Bare GA	Bare GI	NS-CRCA	NS-GA	NS-GI
Log  Z , Ohm.cm <sup>2</sup>	0.36 × 10 <sup>3</sup>	0.75 × 10 <sup>3</sup>	1.14 × 10 <sup>3</sup>	6.28 × 10 <sup>3</sup>	5.16 × 10 <sup>3</sup>	1.13 × 10 <sup>3</sup>
R <sub>p</sub> , Ohm.cm <sup>2</sup>	2.46	2.86	2.95	3.79	3.70	3.05
C <sub>c</sub> , F/cm <sup>2</sup>	1.53 × 10 <sup>-4</sup>	1.11 × 10 <sup>-4</sup>	1.93 × 10 <sup>-4</sup>	0.11 × 10 <sup>-4</sup>	0.12 × 10 <sup>-4</sup>	0.19 × 10 <sup>-4</sup>



**Fig. 12: Comparison of electrochemical impedance spectroscopy of nanostructured coated samples with chromated samples in 3.5% NaCl solution**

V to 1.0 V and - 0.9 V to - 0.5 V, respectively. The polarization resistance ( $R_p$ ) derived from TAFEL plot is given in Table 4 using equation (2). The protection efficiency of NS coatings over the bare substrates (CRCA, GA, and GI) was calculated by using the polarization resistance data as per Table 4 and equation (1). So, in the case of polarization results, the protection efficiency of NS coatings over bare substrates (CRCA, GA, and GI) are 18.2 %, 1.2 %, and 2.8 %, respectively.

$$Polarization\ resistance(R_p) = \frac{(b_a \times b_c)}{2.303 \times I_{corr}(b_a + b_c)} \times 100 \tag{2}$$

In addition to significant reduction in passivation current density, it was revealed that nanostructured coating provides better protective behavior against progress of ions/water compared to others. We also observed from contact angle measurement that nanostructured coating enhances contact angle (> 90°), thereby making the surface energy low. So, water would not adhere to the coating surface. It was also confirming the literature reported data that inhomogeneous

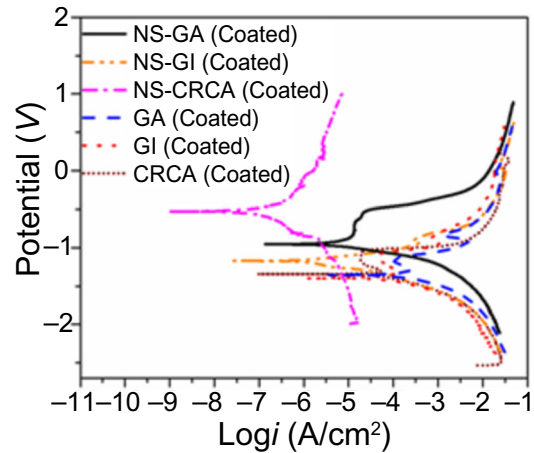


**Fig. 13: Potentiodynamic measurement of different samples in 3.5% NaCl solution**

topological properties without sharp edges of grown zinc oxide nanostructure do not provide sites for water adsorption.<sup>38</sup> By analyzing the above results, we could anticipate a protection mechanism by our bilayer concept where the metal corrosion occurs due to the adsorption of water molecules on the surface followed by the penetration of the corrosive ions into the coating and reaches at the interface of the coating and the substrate.<sup>39</sup> The above ions can initiate the corrosion process. To avoid the diffusion of corrosive ions, suitable coating materials are required to develop on the metal surface, which can suppress the redox reactions/corrosion. Subsequently, the developed hydrophobic and passivating bilayer coating diminished absorption of water molecules on the steel surfaces due to inhomogeneous surface morphology and resulted in a considerable protection from the corrosion process. The above protection was improved when the coating was applied on the ZnO nanostructured mild steel. The presence of inhomogeneous morphological zinc nanostructures in conjunction with the amine-terminated silane molecules considerably lowered the surface energy as well as made the surface more passive; therefore, water contact angle has increased to 97° which in turn improved surface hydrophobicity, and the presence of passivating film showed good anti-corrosion.

**Table 4: Electrochemical data for different samples in 3.5% NaCl solution by DC polarization fittings**

Sample	$E_{\text{corr}}$ (V)	$I_{\text{corr}}$ ( $\mu\text{A}/\text{cm}^2$ )	$b_a$ (V/decade)	$b_c$ (V/decade)	Corrosion rate (mpy)	Polarization resistance ( $R_p$ )
CRCA	– 1.340	26.00	1.000e15	0.149	15.37	2.49E-03
GA	– 1.350	184.0	1.000e15	0.175	108.9	0.41E-03
GI	– 1.400	180.0	1.000e15	0.198	106.5	0.47E-03
NS-CRCA	– 0.527	0.472	0.846	1.189	0.215	455E-03
NS-GA	– 0.954	6.380	0.344	0.105	2.914	5.48E-03
NS-GI	– 1.170	2.210	0.136	0.144	1.305	13.7E-03

## Conclusions

Here, we have developed a method to generate a bi-layer coating over different flat steel substrates, a universal coated product with widespread structural as well as automotive applications, which can be an alternate coating system to carcinogenic and ecotoxic hexavalent chromate passivating layer. It can be scaled up to larger surface area. The coating development steps involve the chemical dipping of steel substrates to obtain the nanostructured ZnO arrays, which can be readily integrated within a top polymer and/or sol-gel layer, using tetraethyl orthosilicate (TEOS) and poly(dimethylsiloxane), bis(3-aminopropyl)-terminated (PDMS-NH<sub>2</sub>) and finally curing at 100°C for 1 to 2 min. The formation of ZnO-NS on steel substrate was confirmed by XRD analysis. Our experimental studies showed lower corrosion rate in polarization measurement and high modulus impedance in electrochemical impedance in 3.5% NaCl solution. The bi-layer thus obtained is more robust in nature and lowers surface energy by enhancing contact angle. Therefore, it does not allow water to adsorb on the surface for making any ionic diffusion path to penetrate into the coating interface.

**Acknowledgment** Authors are thankful to Tata Steel management for allowing us to carry out the present work. We are extending our thanks to Ms Nitu Rani, Ms Puja Kumari, Ms Samvedana, Mr. Vikram Sharma, Ms Puspanjali Mohanta, Ms Priyanka Pandey, and Mr. Arup Kumar Halder for helping in the experimental measurements. We are also grateful to laboratory staff of department of applied chemistry and department of applied physics of IIT (ISM) Dhanbad, India for helping us to carry out the wet chemical experiments.

## References

- Marmur, A, “The Lotus Effect: Superhydrophobicity and Metastability.” *Langmuir*, **20** (9) 3517–3519 (2004)
- Lee, HJ, Michielsen, S, “Lotus Effect: Superhydrophobicity.” *J. Text. Inst.*, **97** (5) 455–462 (2006)
- Von Baeyer, HC, “The Lotus Effect.” *Sciences*, **40** (1) 12–12 (2000)
- Zhou, CJ, Tian, D, He, JH, “What Factors Affect Lotus Effect.” *Therm. Sci.*, **22** (4) 1737–1743 (2018)
- Latthe, SS, Sutar, RS, Kodag, VS, Bhosale, AK, Kumar, AM, Sadasivuni, KK, Xing, R, Liu, S, “Self-Cleaning Superhydrophobic Coatings: Potential Industrial Applications.” *Progress Organ. Coat.*, **128** 52–58 (2019)
- Samaha, MA, Tafreshi, HV, Gad-el-Hak, M, “Superhydrophobic Surfaces: From the Lotus Leaf to the Submarine.” *Comptes Rendus Mécanique*, **340** (1–2) 18–34 (2012)
- Guin, AK, Nayak, S, Rout, TK, Bandyopadhyay, N, Sengupta, DK, “Corrosion Resistance Nano-Hybrid Sol–Gel Coating on Steel Sheet.” *ISIJ Int.*, **51** (3) 435–440 (2011)
- Kumar, PS, Sundaramurthy, J, Mangalaraj, D, Nataraj, D, Rajarathnam, D, Srinivasan, MP, “Enhanced Superhydrophobic and Switching Behavior of ZnO Nanostructured Surfaces Prepared by Simple Solution–Immersion Successive Ionic Layer Adsorption and Reaction Process.” *J. Colloid Interface Sci.*, **363** (1) 51–58 (2011)
- Amirshaqai, N, Salami-Kalajahi, M, Mahdavian, M, “Corrosion Behavior of Aluminum/Silica/Polystyrene Nanostructured Hybrid Flakes.” *Iran. Polym. J.*, **23** (9) 699–706 (2014)
- Jayakumar, N, Veedu, KK, Gopalan, NK, “Durable Hydrophobic Coating Based on Cerium Phosphate Nanorod-siliconized Epoxy for Corrosion Protection.” *ACS Appl. Nano Mater.*, **2** (5) 2689–2696 (2019)
- Joula, MH, Farbod, M, “Synthesis of Uniform and Size-Controllable Carbon Nanospheres by a Simple Hydrothermal Method and Fabrication of Carbon Nanosphere Superhydrophobic Surface.” *Appl. Surface Sci.*, **347** 535–540 (2015)
- Larmour, IA, Bell, SEJ, Saunders, GC, “Remarkably Simple Fabrication of Superhydrophobic Surfaces Using Electroless Galvanic Deposition.” *Angew. Chem. Int. Ed.*, **46** (10) 1710–1712 (2007)
- Cao, L, Lu, X, Pu, F, Yin, X, Xia, Y, Huang, W, Li, Z, “Facile Fabrication of Superhydrophobic Bi/Bi<sub>2</sub>O<sub>3</sub> Surfaces with Hierarchical Micro-Nanostructures by Electroless Deposition or Electrodeposition.” *Appl. Surface Sci.*, **288** 558–563 (2014)
- Smielak, B, Klimek, L, “Effect of Hydrofluoric Acid Concentration and Etching Duration on Select Surface Roughness Parameters for Zirconia.” *J. Prosthetic Dentistry*, **113** (6) 596–602 (2015)
- Zareidoost, A, Yousefpour, M, Ghaseme, B, Amanzadeh, A, “The Relationship of Surface Roughness and Cell Response of Chemical Surface Modification of Titanium.” *J. Mater. Sci. Mater. Med.*, **23** (6) 1479–1488 (2012)
- Wang, T, Zhao, X, Yang, H, Qi, Y, “On the Roles of HEC in Pechini Sol-Gel Method: Enhancement of Stability, Wettability

- bility of the Sol and Surface Roughness of Bi2212 Film.” *Ceram. Int.*, **44** (11) 12144–12148 (2018)
17. Dillip, GR, Banerjee, AN, Anitha, VC, Joo, SW, Min, BK, Sawant, SY, Cho, MH, “Anchoring Mechanism of ZnO Nanoparticles on Graphitic Carbon Nanofiber Surfaces Through a Modified Co-precipitation Method to Improve Interfacial Contact and Photocatalytic Performance.” *Chem-PhysChem*, **16** (15) 3214–3232 (2015)
  18. Rafique, MS, Tahir, MB, Rafique, M, Shakil, M, “Photocatalytic Nanomaterials for Air Purification and Self-cleaning.” *Nanotechnol. Photocatal. Environ. Appl.*, **12** 203–219 (2020)
  19. Zhao, J, Luo, H, Wang, L, Li, W, Zhou, T, Rong, B, “TEOS/PDMS-OH Hybrid Material for the Consolidation of Damaged Pottery.” *Herit. Sci.*, **1** (1) 1–10 (2013)
  20. Gong, X, He, S, “Highly Durable Superhydrophobic Polydimethylsiloxane/Silica Nanocomposite Surfaces with Good Self-cleaning Ability.” *ACS Omega*, **5** (8) 4100–4108 (2020)
  21. Guan, F, Song, Z, Xin, F, Wang, H, Yu, D, Li, G, Liu, W, “Preparation of Hydrophobic Transparent Paper via Using Polydimethylsiloxane as Transparent Agent.” *J. Bioresour. Bioprod.*, **5** (1) 37–43 (2020)
  22. Hasanzadeh, M, Far, HS, Haji, A, Rosace, G, “Facile Fabrication of Breathable and Superhydrophobic Fabric Based on Silica Nanoparticles and Amino-Modified Polydimethylsiloxane.” *Preprints*, 2020050123 (2020).
  23. Tse, CW, Leung, YH, Tam, KH, Chan, WK, Djuricic, AB, “Tailoring and Modifications of a ZnO Nanostructure Surface by the Layer-by-Layer Deposition Technique.” *Nanotechnology*, **17** (14) 3563–3568 (2006)
  24. Guin, AK, Nayak, SK, Rout, TK, Bandyopadhyay, N, Sengupta, DK, “Corrosion Behavior of Nanohybrid Titania–Silica Composite Coating on Phosphated Steel Sheet.” *J. Coat. Technol. Res.*, **9** (1) 97–106 (2012)
  25. Guin, AK, Nayak, S, Bhadu, MK, Singh, V, Rout, TK, “Development and Performance Evaluation of Corrosion Resistance Self-healing Coating.” *Int. Sch. Res. Not.*, **2014** 1–7 (2014)
  26. Velazquez, JM, Baskaran, S, Gaikwad, AV, Ngo-Duc, T-T, He, X, Oye, MM, Meyyappan, M, Rout, TK, Fu, JY, Banerjee, S, “Effective Piezoelectric Response of Substrate-Integrated ZnO Nanowire Array Devices on Galvanized Steel.” *ACS Appl. Mater. Interfaces*, **5** (21) 10650–10657 (2013)
  27. Zak, AK, Razali, R, Majid, WH, Darroudi, M, “Synthesis and Characterization of a Narrow Size Distribution of Zinc Oxide Nanoparticles.” *Int. J. Nanomed.*, **6** 1399–1403 (2011)
  28. Riehle, N, Gotz, T, Kandelbauer, A, Tovar, G, Lorenz, G, “Data on the Synthesis and Mechanical Characterization of Polysiloxane-Based Urea-Elastomers Prepared from Amino-Terminated Polydimethylsiloxanes and Polydimethyl-Methyl-Phenyl-Siloxane-Copolymers.” *Data Brief*, **18** 1784–1794 (2018)
  29. Johnson, LM, Gao, L, Wyatt, SIVC, Smith, M, Efimenko, K, “Elastomeric Microparticles for Acoustic Mediated Bioseparations.” *J. Nanobiotechnol.*, **11** (1) 1–8 (2013)
  30. Shamsodin, M, Fazli, M, Nasiri, M, “Comparison Study of Paraquat Herbicide Adsorption by Xerogels: Application of Experimental Design.” *Environ. Progress Sustain. Energy*, **38** (s1) S128–S138. <https://doi.org/10.1002/ep.12947> (2019)
  31. Chitra, K, Annadurai, G, “Fluorescent Silica Nanoparticles in the Detection and Control of the Growth of Pathogen.” *J. Nanotechnol.*, 2013 (2013)
  32. Wencel, D, Dolan, C, Barczak, M, Keyes, TE, McDonagh, C, “Synthesis, Tailoring and Characterization of Silica Nanoparticles Containing a Highly Stable Ruthenium Complex.” *Nanotechnology*, **24** (36) 365705 (2013)
  33. Nuraini, L, Triwulandari, E, Ghazali, M, Hanafi, M, Jumina, J, “Synthesis of Polyurethane/Silica Modified Epoxy Polymer Based on 1, 3-Propanediol for Coating Application.” *Indonesian J. Chem.*, **17** (3) 477–484 (2017)
  34. Kobayashi, S, “IR Spectroscopic Study of Silicon Nitride Films Grown at a Low Substrate Temperature Using Very High Frequency Plasma-Enhanced Chemical Vapor Deposition.” *World J. Condens. Matter Phys.*, **6** (4) 287–293 (2016)
  35. Zhang, D, Wang, L, Qian, H, Li, X, “Superhydrophobic Surfaces for Corrosion Protection: A Review of Recent Progresses and Future Directions.” *J. Coat. Technol. Res.*, **13** (1) 11–29 (2016)
  36. Rout, TK, Jha, G, Singh, AK, Bandyopadhyay, N, Mohanty, ON, “Development of Conducting Polyaniline Coating: A Novel Approach to Superior Corrosion Resistance.” *Surf. Coat. Technol.*, **167** (1) 16–24 (2003)
  37. Rout, TK, Bandyopadhyay, N, Venugopalan, T, Bhattacharjee, D, “Mechanistic Interpretation of Electrochemical Behaviour of Galvannealing Coating in Saline Environment.” *Corros. Sci.*, **47** (11) 2841–2854 (2005)
  38. Rawal, TB, Ozcan, A, Liu, SH, Pingali, SV, Akbilgic, O, Tetard, L, O’Neill, H, Santra, S, Petridis, L, “Interaction of Zinc Oxide Nanoparticles with Water: Implications for Catalytic Activity.” *ACS Appl. Nano Mater.*, **2** (7) 4257–4266 (2019)
  39. Ibrahim, M, Kannan, K, Parangusan, H, Eldeib, S, Shehata, O, Ismail, M, Zarandah, R, Sadasivuni, KK, “Enhanced Corrosion Protection of Epoxy/ZnO-NiO Nanocomposite Coatings on Steel.” *Coatings*, **10** (8) 783 (2020)

**Publisher’s Note** Springer Nature remains neutral with regard to jurisdictional claims in published maps and institutional affiliations.